Acta Geotechnica (2024) 19:1477–1494
https://doi.org/10.1007/s11440-023-02004-1

RESEARCH PAPER

Lesson learnt from static pulling tests on trees: an experimental study on toppling behaviour of complex foundations

Andrea Galli[1] · Cristian Sala[2,3] · Riccardo Castellanza[3] · Andrea Marsiglia[2,4] · Matteo Oryem Ciantia[4]

Received: 14 April 2022 / Accepted: 9 July 2023 / Published online: 1 August 2023

Abstract

Standard procedures for stability assessment of unstable trees are based, among other, on the interpretation of on-site, non-destructive static pulling tests. To this goal, a simple phenomenological equation is usually adopted in professional agronomic practice, and an estimation of the ultimate toppling resistance is extrapolated by fitting the test data, without taking root geometrical parameters and soil mechanical properties into account. From a geotechnical point of view, however, the root plate of a tree plays the role of a "living foundation", and its behaviour under toppling actions (like those produced by intense wind gusts) conceptually corresponds to the mechanical response of shallow foundations under rocking loads. In the paper, several static pulling tests on real-scale trees (some of them have been run until the complete collapse, after some unloading–reloading cycles) and some tests taken from the literature are considered in order to investigate the toppling behaviour. A possible new interpretative equation is proposed and critically compared with the existing one against experimental results. The new equation allows for a mechanically meaningful description of the toppling curve of the tree and accounts for strength and deformability issues. It allows to introduce innovative "performance-based" approaches, which are commonly neglected by practitioners and professional agronomists in this field. Nevertheless, the experimental results show that tree toppling is a complex phenomenon, and capturing its failure condition requires more advanced multi-mechanism models and second-order effects to be accounted for. From a practical point of view, the proposed equation, employed within the same standard interpretative procedure currently adopted in practice for pulling tests, seems to provide conservative estimations of "operational" values of the ultimate toppling resistance, and in perspective, it could be used to significantly optimize—when needed—the design of structural stabilizing interventions on potentially unstable trees.

Keywords Experimental results · Foundations · Performance-based approaches · Pulling tests · Stability of trees

1 Introduction

The interest towards tree stability assessment and, more in general, arboreal heritage protection is rapidly increasing in modern societies. It represents a key issue for the management of urban areas, where accurate analysis techniques can substantially help in protecting both natural heritage (e.g. monumental and historic trees) and human activities. Trees also play an important role as sustainable drainage systems in urban areas, thus mitigating the risk associated with rainfall-induced flooding events [25, 24]. Sudden tree collapse may induce severe damage to existing structures or goods, imply the temporarily lack of serviceability of infrastructures and even cause the loss of human lives. Lack of monitoring and maintenance

✉ Andrea Galli
andrea.galli@polimi.it

[1] Department of Civil and Environmental Engineering, Politecnico di Milano, Piazza Leonardo da Vinci 32, 20133 Milano, Italy

[2] Agro Service S.r.l., Cormano, Italy

[3] Department of Earth and Environmental Sciences, Università Degli Studi Milano Bicocca, Milano, Italy

[4] School of Science and Engineering, University of Dundee, Dundee DD1 4HN, UK

interventions, joint to the more and more intense wind gusts induced by climate changes, also contribute to increase the emergency about the stability of trees. Tree risk assessment is hence becoming part of general risk management analyses, and as such, it requires specific risk mitigation strategies [1, 4].

In forest regions, the protection of arboreal heritage is strictly related to biomass conservation, biodiversity promotion, soil erosion control and stability of slopes. Recent events have shown that also in these regions trees are exposed to a marked risk. For example, the 2018 Mediterranean storm Adrian caused the loss of 6 to 8 million of cubic metres of wood of standing trees (just considering the Italian region), the death of 14 people [19] and more than €3.3 billion in damages (https://www.aon.com/). Also storm Arwen in November 2021 saw extreme winds hit the UK, causing large-scale damage, several fatalities and cascading impacts to utilities, services and across many of Scotland's forests. It is understood that 8,000 hectares of woodland (an estimated 16 million trees) was blown down during Storm Arwen [2].

More in general, climate change is likely to impact significantly the basic transport infrastructures and the built environment worldwide due to a more arid, erratic and storm-prone weather pattern [27]. As vegetation by itself is a carbon sink, it is thus increasingly urgent to protect and manage existing green heritage and further develop low-carbon stabilization measures, such as the use of vegetation in geotechnical engineering design. In ground bioengineering, for example, living plant material is employed to perform engineering functions [32]. Since the pioneering work of [28], there are many well-documented examples in which plants have been used for ground stabilization. However, uptake and development of this technology have been very slow [33] because of the difficulty engineers face when trying to quantify the beneficial effects of vegetation in design practice [18]. That difficulty arises because of the complexity of the involved phenomena [16], the relative scarcity of systematic experimental data and the limitations of modelling tools [32].

Within the aforementioned bioengineering context, however, stability assessment of trees requires a deep change in the interpretative perspective, since in this case the attention needs to be addressed to the anchoring strength of the root systems within the soil, rather than on its average reinforcing effect on the representative soil volume. In this context, the paper investigates the behaviour of the root system of a tree, conceptually assimilated to the foundation of a slender structure (e.g. a column or a smokestack) "anchored" within the soil, and subject to rocking loads, as those induced by wind gusts.

In the last twenty years, the approaches usually adopted to assess the state of trees have evolved from the traditional Visual Tree Assessment (VTA; [17]), towards the use of quantitative geometry-based indexes, such as the slenderness ratio of the tree. More recently, traditional concepts from geotechnical and structural engineering (like equilibrium and compatibility equations, together with proper failure criteria) have also been included in stability assessment procedures of a tree, thought as a "natural" and living structure [26].

Early experimental studies on real-scale trees tried to relate the stability of the tree to its mechanical and geometrical properties, focusing, for example, on sway frequency [15, 30] or on the value of the maximum resisting toppling moment [7]. Advanced small-scale tests on tree models have also been performed, for example, by considering wind tunnel facilities [5, 14] or geotechnical centrifuge tests [39, 38].

With the aim of defining valuable predictive models, simplified descriptions of the roots architecture and of their biomechanical properties are in general considered [3], and their strengthening effects on the toppling failure mechanism can be derived by properly considering the pull-out resistance of the root [29].

More recently, advanced finite element numerical models [9, 36, 37] have also been used to reproduce the experimental results. [8] recently extended the traditional macroelement approach for shallow foundations [21] to model the mechanical behaviour of tree roots soil systems. The same approach was used by [39] to correct centrifuge data and compare results with the field test data by [10] and [20]. The good comparison between the results suggests that a macroelement approach can be a promising modelling framework to evaluate the stability of trees.

Despite all the aforementioned scientific developments, in standard agronomic practice the toppling resistance of trees is commonly based on VTA or on-site non-destructive tests. Among others, static pulling tests are widely used to get an estimation of the toppling resistance of the tree against global uprooting failure mechanisms. Pulling tests actually bypass the problem of a detailed characterization of the root geometry and of the soil, and predictions are obtained via a phenomenological interpretation of the experimental data, based on the procedure proposed by Wessolly and Erb [34] and briefly described in Sect. 2. Such procedure was calibrated on a rich database of experimental pulling tests, run on trees with a diameter between 15 and 35 cm until the complete toppling, and identified a common interpolating equation.

Albeit the Wessolly and Erb equation is largely adopted in practice, the need of a more accurate fitting equation will be clearly put in evidence here below with respect to some pulling tests taken from the literature. Some intrinsic as well as conceptual limitations will be pointed out and a more general interpretative equation will be proposed

(without significant additional computational costs for the final user), allowing to derive some significant observations about the mechanical behaviour of the system. Validations against a series of real pulling tests to failure are also presented in the paper, and the results critically compared to the Wessolly and Erb approach. One small-scale experimental tests will finally also be used to assess the moment–rotation curve predicting capability in a more controlled laboratory environment.

Independently of the chosen analytical formulation, the proposed interpretative framework could not only increase the accuracy in tree stability assessment for practical on-site applications, but, from a modelling point of view, it could provide essential information for the development of more reliable engineering models, based, for example, on macroelement approaches specifically conceived for trees.

2 The Wessolly and Erb model for interpreting pulling tests

Pulling tests are usually executed by applying on a tree a force F at a height H and with an inclination α with respect to the horizontal ground surface, and by recording the corresponding rotation φ of the base of the trunk (Fig. 1a). The aforementioned Wessolly and Erb procedure is based on the numerical fitting of the experimental data by means of the following equation.

$$\varphi = \frac{1}{3}\tan\left(\frac{100}{73,85}\frac{F}{F_L}\right) + \frac{1}{2}\left(\frac{F}{F_L}\right)^2 - \frac{1}{10}\frac{F}{F_L}, \quad (1)$$

where the parameter F_L represents the limit value of the force F, ideally corresponding with the limit toppling resistance of the tree. The trend of Eq. (1) together with the fan of variability of the experimental results of [34] is shown in Fig. 1b. In order to prevent possible damage to the roots, the test is usually limited to maximum rotations not exceeding 0.2°, which corresponds to a very limited portion of the curve, and the value of F_L is then obtained as extrapolation over the measured data.

Over the years, Eq. (1) has been widely employed for professional activities in agronomic practice and got several experimental confirmations (an accuracy ranging from ± 4% to about ± 37% on the evaluation of F_L was reported by [31] on the basis of twelve field tests).

Several critical observations can, however, be expressed:

(a) the introduction of only one fitting parameter (F_L) allows to scale the curve only with respect to the load axis (i.e. the axis F/F_L) and implicitly assumes the value $\varphi_L = 1.914°$ (see Fig. 1b) as "the" limit rotation for a tree, independently from the geometrical and mechanical characteristics of the system;
(b) similarly, Eq. (1) does not allow to precisely fit the initial roundness of the experimental curve, thus potentially making largely inaccurate any extrapolation with respect to the measured data;
(c) no reference is in general made to the type of soil interacting with the root system;
(d) the limited range of diameters considered in the calibration (15–35 cm) makes it hardly applicable to larger-diameter trees, which represent however a

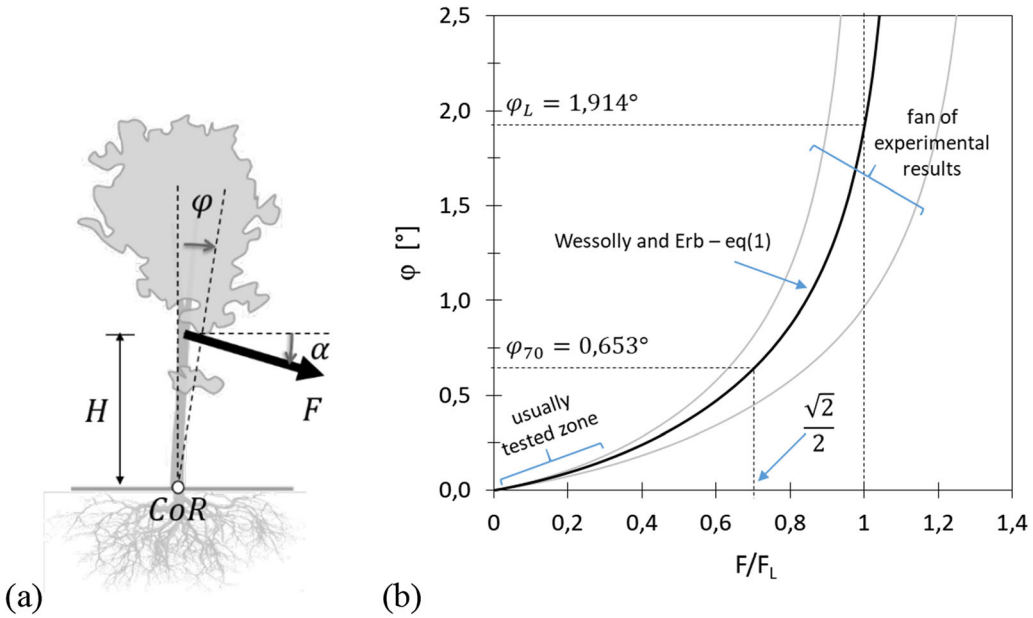

Fig. 1 **a** Schematic view of a pulling test; **b** Wessolly and Erb curve (solid line)

class of trees frequently studied in practical applications (like in the case of monumental or historic trees).

From a mechanical point of view, moreover, it can be also noted that Eq. (1).

(e) does not show any asymptotic trend when F approaches F_L, as it should derive from a consistent definition of a limit failure condition for a perfect ductile system;

(f) does not represent a meaningful mechanical relationship, since it is expressed in terms of static and kinematic variables (F and φ, respectively) which are not work-conjugate to each other; as a consequence, no further interpretations (like the definition of a representative global rotational stiffness or the evaluation of the dissipated energy during the test) can be derived;

(g) does not allow an explicit mathematical inversion, thus making it hardly applicable in displacement-controlled numerical models.

In particular, points (a), (c) and (f) are of fundamental importance in view of possible extensions of the study, like (i) the application to large-diameter trees, (ii) the search for meaningful correlations with well-defined soil mechanical properties, (iii) the investigation of more complex loading conditions (dynamic effects of wind gusts, seismic actions, etc.) and (iv) the comparison with advanced numerical modelling approaches (e.g. 3D finite element simulations).

3 Proposition of a new interpolating equation

From a mechanical point of view, the pulling test sketched in Fig. 1a can be assimilated to a toppling test on a single-d.o.f. rotational system, described by a rotation φ with respect to its centre of rotation (*CoR*, assumed to coincide with the base of the trunk), under an applied moment M computed as:

$$M = H \cdot F \cdot \cos\alpha. \tag{2}$$

Hereafter, a new physically based equation is proposed:

$$\frac{M}{M_L} = \left[\frac{2}{\pi}\arctan\left(a\frac{\varphi}{\varphi_{70}}\right)\right]^b \text{with } a = \tan\left[\frac{\pi}{2}\left(\frac{\sqrt{2}}{2}\right)^{1/b}\right], \tag{3}$$

where moment values M are expressed as a function of the trunk rotation φ, and an additional shape parameter, represented by the exponent b, have been added to the arctangent function. Equation (3) was inspired by Eq. (1), by removing all the polynomial terms and inverting the tangent relationship, and by introducing a scaling parameter for tree rotations. In Eq. (3) the toppling moment M (static quantity) takes the place of the applied pulling force F, and it is directly linked with its work-conjugate kinematic quantity, i.e. the rotation φ measured in the pulling plane (the plane defined by the direction of applied force F and by the centre of rotation, *CoR*). This new equation represents then a meaningful mechanical relationship, characterized by three parameters. In particular, M_L corresponds with the limit asymptotic resistance of the root system against toppling, and φ_{70} represents a reference rotation angle of the system, corresponding to an applied toppling moment $M_{70} = \frac{\sqrt{2}}{2}M_L$ (i.e. about 70% of M_L). Exponent b, finally, controls the roundness of the curve, in particular for very limited rotation amplitudes. It is worth noting that the term a is an internal parameter, uniquely dependent on b and introduced here only for the sake of clarity of the analytical expression. Its definition derives from imposing $M/M_L = \sqrt{2}/2$ when $\varphi = \varphi_{70}$.

A parametric study of Eq. (3) is shown in Fig. 2, together with a consistent non-dimensional plot of Eq. (1). This latter was in particular obtained by normalizing the rotation axis φ with respect to the corresponding φ_{70} value derived for Wessolly and Erb Eq. (0.653°, as defined in Fig. 1a), and, owing to Eq. (2), by equivalently expressing the ratio F/F_L as M/M_L. Figure 2 highlights in particular the influence of the exponent b on the roundness of the proposed curve for limited rotations ($\varphi/\varphi_{70} < 1$), where Eq. (3) tends to coincide with Wessolly and Erb equation when $b \cong 1$. Values of $b > 1$ would instead induce an upward concavity of the curve and they cannot be accepted. For larger rotations ($\varphi/\varphi_{70} > 1$), a clear asymptotic trend is evident in Eq. (3), and parameter b does not significantly affect any longer the curve.

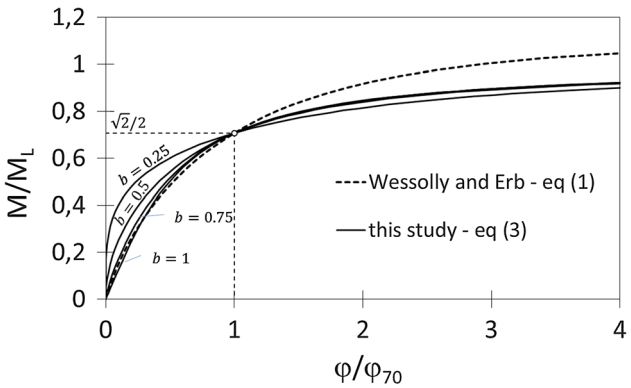

Fig. 2 Parametric study of Eq. (2) and comparison with a dimensionless Wessolly and Erb curve

3.1 Comparison on experimental data from the literature

The two equations were firstly tested on some experimental test results available from the literature, whose details are listed in Table 1. In particular, three tests on *Larix europea* ([6]; labelled as #1, #2 and #3) and five tests on *Pinus pinaster* ([10]; labels have been here chosen consistently with the cited paper) have been considered in Figs. 3 and 4, respectively, and compared with fitting data from Eqs. (1) and (3).

In both cases, Eq. (1) does not allow for a precise fitting of the data, since it does not allow to rescale the curves along the φ axis. A simple parametrical analysis on the values of parameter M_L is only shown (dashed lines in Figs. 3a and 4a) for a qualitative comparison with the experimental curves. On the contrary, Eq. (3) shows a very good fitting capability (full lines in Figs. 3b and 4b). In both cases, the least square method has been applied. The pre-peak branch only of the curves was considered during the fitting procedure, since the proposed equation is not intended to reproduce also the post-peak response. For the sake of completeness, the values of the fitting parameters for Eq. (3) are also listed in Table 1.

3.2 A remark on parameter φ_{70}

At authors' judgement the introduction of parameter φ_{70} is of particular mechanical interest, since it represents the rotation of the tree under a fixed reference working condition (about 70% of M_L). It can be thought then as a measure of the "performance" of the system, and for practical applications, it could extend the criteria for evaluating the stability of a tree. These latter are in fact currently based on standard "capacity-based" criteria, comparing the expected working condition (i.e. a "design" applied moment M_d) to the ultimate toppling resistance M_L by introducing a global safety factor $F_S = M_L/M_d$. Such definition, evidently, completely neglects deformability issues, which can, however, play a fundamental role when the rocking behaviour of tall structures is concerned. Important trunk rotations can in fact induce remarkable second -order effects, related, for example, to the weight of the crown or to excessive damage associated with the pull-out behaviour of the thinnest roots. Trees characterized by similar values of M_L, but by remarkably different values of φ_{70} should be then associated with different evaluations in terms of overall stability against toppling. This implies, for example, that acceptability criteria for the values of global safety factor F_S (values between 1.3 and 1.5 are usually accepted in practice) cannot be a priori fixed, but they should depend also on φ_{70} values. From a conceptual point of view, the introduction of a performance parameter like φ_{70} allows to move from traditional "capacity-based" to the so called "performance-based" approaches, as it already happens in several fields of geotechnical and civil engineering [12, 13, 22, 23].

4 Experimental pulling tests

4.1 Test sites

Following the loading scheme sketched in Fig. 1a, during this study several pulling tests were run on real-scale trees. Four of them (tests A, B, C and D in the following) were conducted on relatively large-diameter trees, according with the standard non-destructive approach, consisting in a single loading phase not exceeding a rotation of about 0.2°. The tests were controlled by professional agronomists and they were stopped before inducing irreversible damages to the trees. For the sake of clarity, a picture of the

Table 1 List of parameters for pulling tests reported in Figs. 3 and 4

Source	Type of soil	Type of tree	Diameter [cm]	Tree height [m]	Test label	M_L [kNm]	φ_{70} [°]	b [−]
Crook and Ennos [6]	sandy clay loam	Larix europea	12–20	10–13	#1	12.76	11.15	1.00
					#2	17.71	9.40	1.00
					#3	30.17	28.66	1.00
Dèfossez et al. [10]	medium sand	Pinus pinaster	17.98	10.62	#14	17.33	5.41	1.00
			18.46	10.40	#15	15.83	5.29	0.78
			16.87	9.70	#31	14.21	4.27	1.00
			16.87	9.68	#32	12.19	5.47	1.00
			16.55	10.65	#36	8.95	6.37	0.96

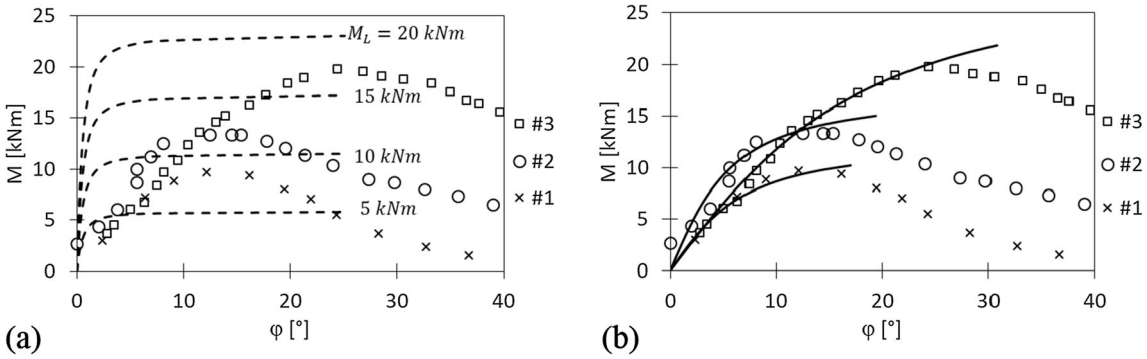

Fig. 3 Fitting on test results from [6] with **a** Eq. (1) and **b** Eq. (3)

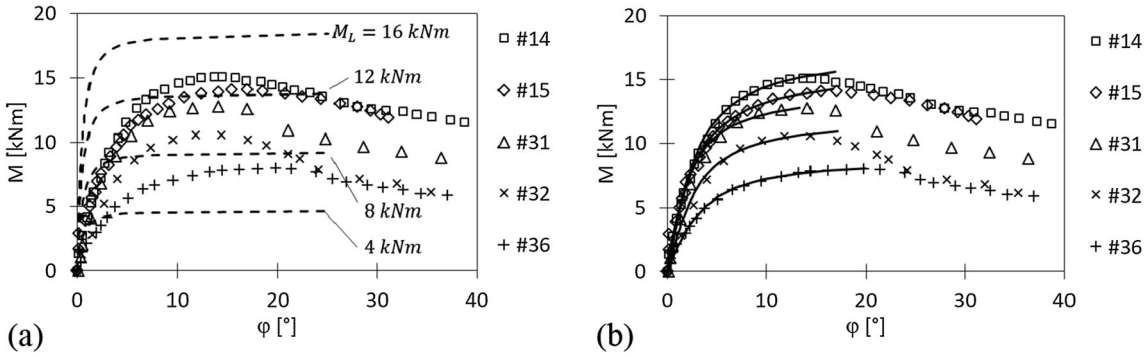

Fig. 4 Fitting on test results from [10] with **a** Eq. (1) and **b** Eq. (3)

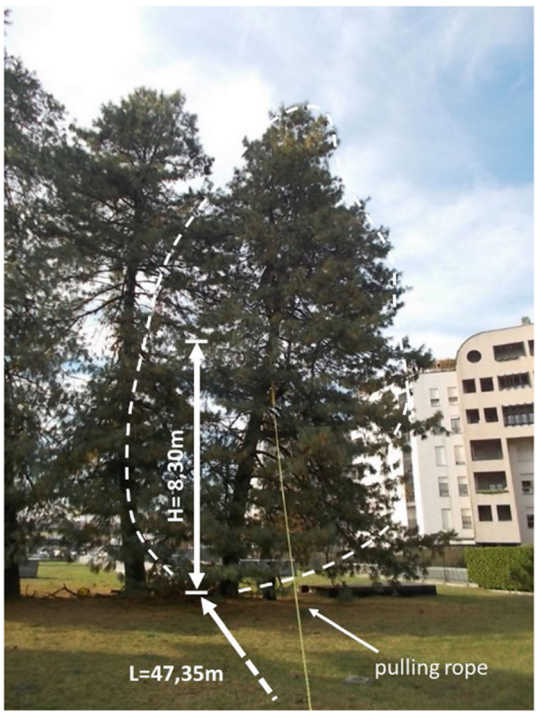

Fig. 5 Experimental set up of test A

experimental set up of test A is shown in Fig. 5; Table 2 summarizes the tree typologies and the main geometrical characteristics for all the tests, where D is the trunk diameter, H is the elevation above ground of the pulling rope and L is the distance of the tested tree from the ground anchoring point.

Table 2 Tree typologies and geometrical characteristics of the experimental tests

Test	Type of tree	Diameter D [cm]	Pulling height H [m]	Anchoring distance L [m]
A	Pinus wallichiana	70	8.3	47.35
B	Cedrus deodara	101	11.5	33.1
C	Cupressus arizonica	43	4	19
D	Liriodendron tulipifera	70	10.5	22.95
E	Prunus avium	22	0.4	16.8
F	Robinia pseudoacacia	30	4.6	39.50

Two other tests (tests E and F in the following) were on the contrary run on smaller-diameter trees (within the range 15–35 cm, consistently with the calibration of Wessolly and Erb equation), but followed a non-standard loading path, consisting in several loading–unloading cycles at

increasing amplitude until the failure, thus mimicking (although in a quasistatic scheme) the effects of horizontal wind gusts.

For the sake of brevity, the results of the standard pulling tests A, B, C and D are discussed directly in Sect. 5.1, whilst, on the contrary, a detailed description of the two non-standard tests E and F is separately reported in Sects. 4.4 and 4.5, respectively. A seventh experimental tests was in addition chosen from the literature data [8], with reference to a 1:20 small-scale 1-g pulling test on a model tree, in order to test the capability of Eqs. (1) and (3) to capture also remarkable size effects (see Sect. 5.3 for a brief description).

4.2 Loading device and measuring system

The load was applied for all test by means of a manual winch and measured by a commercial load cell (Fig. 6a; maximum capacity 5 tons). Rotations for tests A, B, C and D where measured by means of a commercial small-scale inclinometer (Fig. 6b; measurement range ± 2°; resolution 0.001°), recording the base tree rotation in the pulling plane, whilst for tests E and F a 3-axis large-scale inclinometer was used (Fig. 6c; measurement range ± 90°; resolution 0.05°). This latter was installed with axes x and y laying in the pulling plane (along the horizontal and vertical directions, respectively), whilst axis z represents the main axis of rotation of the test (see also Figs. 8a and 10a). The experimental data were acquired at a frequency of 10 Hz, by using the software provided for the measuring devices.

4.3 Soil description

For both tests E and F, one soil sample was dug at a depth of about 30 cm, at a distance of about 150–170 cm from the trunk. In both cases the soil can be classified as a silty sand, with important gravelly fractions; the two grain size distributions are reported in Fig. 7a, whilst the particle size characterization of the two soil samples is summarized in Table 3.

Standard direct shear tests were also executed on three soil samples (labelled S1, S2 and S3) extracted by means of an excavator within the first metre of the topping soil at a distance of 10 m from the trees (in order not to disturb the root plates). The samples (reconstituted at an average value of the dry unit weight γ_{dry}= 18.09 kN/m^3, and tested under normal confining pressures σ_n' of 100, 200 and 300 kPa in dry conditions; Fig. 7b) showed a global ductile response, with average friction angle value ϕ'=30.9°. The tests were

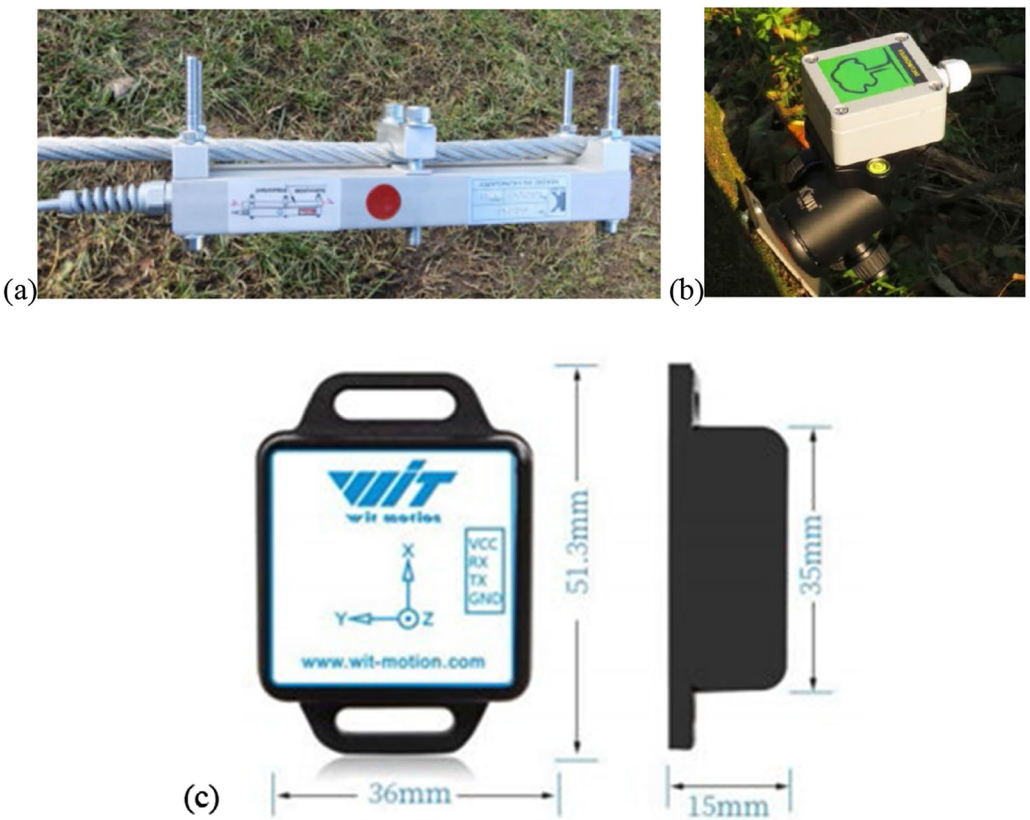

Fig. 6 Adopted instrumental equipment for pulling test: **a** load cell and **b** small-scale inclinometer [11]; **c** 3-axis large-scale inclinometer [35]

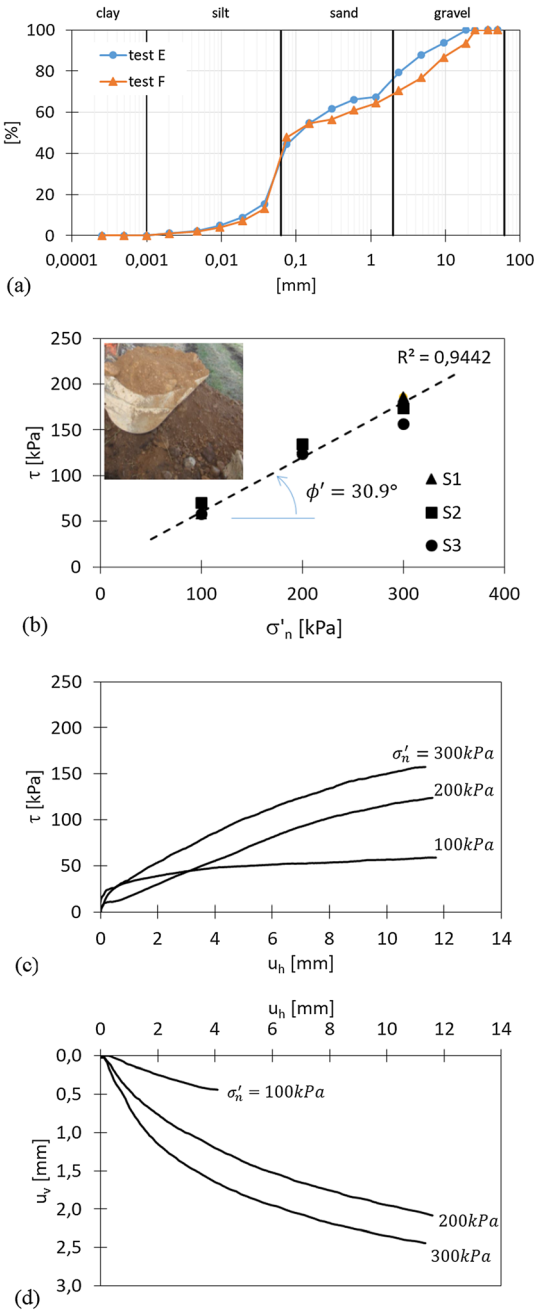

Fig. 7 **a** Grain size distributions of the soil samples for tests E and F; **b** interpretation of direct shear test results on soil samples S1, S2 and S3; **c** shear stress–horizontal displacement curves for the tests on soil sample S3; **d** vertical displacement–horizontal displacement curves for the tests on soil sample S3

conducted at a controlled horizontal displacement rate of about 8 µm/min, on samples with a cross-sectional area of 28.26 cm^2. As an example, for the sake of completeness the trends of the shear stress (τ) and of the vertical displacement (u_v; positive values indicate contractive behaviour) recorded during the tests on sample S3 are also reported as a function of the horizontal displacement (u_h) in Fig. 7c and d, respectively. (The acquisition of u_v values during the test at 100 kPa of confinement was interrupted at about 0.5 mm.) No further geotechnical characterization of these soil samples has been performed, since the aim was here to provide the reader an idea of the basic properties of the soil involved in the tests. Clear relationships of soil mechanical properties with the global toppling behaviour of an entire root plate of a real-scale tree can in fact be found only on the basis of advanced mechanical characterizations of the soil (taking into account unsaturated soil response, mechanical behaviour at very low confining stress, large strain deformations, interaction with the grass roots and other vegetation at shallow depths, etc.). All these data are rarely available for practical applications of standard non-destructive pulling tests and are generally beyond the (time and funds) budgets. The scope of the present paper, on the contrary is to more accurately describe the overall toppling behaviour, and to compare the predicting capabilities of the two Eqs. (1) and (3) when fitting limited ranges of tree rotations data.

4.4 Test E

The test was run on a relatively small tree (diameter of D = 22 cm) that can be considered as an "ideal" case of a healthy tree (the wood did not present any evidence of structural weakness), falling within the range of diameters 15–35 cm. The trunk was previously completely pruned at a height of about 190 cm from the ground in order to prevent any second-order effects related to the weight of the crown to affect the $M - \varphi$ curve, even for large rotation values. The pulling rope was fixed at a height of H = 40 cm from the ground, and it was anchored at the base of another stable tree at a distance of L = 16.8 m (Fig. 8a). The inclination of the applied pulling force F was then very limited (angle α = 1.36°), so that a negligible vertical load component is transferred to the root system. The load program consisted in three loading–unloading cycles (labelled (1), (2) and (3), respectively, whilst the label (0) indicates the start of the loading) at increasing amplitude; recorded values of moment M and rotation φ are plotted in Fig. 8b (a pause of about 30 min between cycles (1) and (2) allowed a preliminary check of the results). The complete toppling of the tree was reached during a following fourth loading phase, whose values have, however, been here omitted since they are out of scale (very large rotations were in fact reached, for which the applied load had a relevant tensile component with respect to trunk direction, rather than only a toppling one). The positions of the tree during the different phases of the loading program are schematically represented in Fig. 8c (solid lines, labelled 0

Table 3 Particle size characterization of the soil samples from tests *E* and *F*, together with the measured values of the soil moisture content w_n

	Clay [%]	Silt [%]	Sand [%]	Gravel [%]	D_{10} [mm]	D_{50} [mm]	D_{60} [mm]	C_U [−]	w_n [%]
Test E	0.02	35.09	40.44	24.45	0.02	0.12	0.26	11.76	27
Test F	0.06	33.88	34.66	31.40	0.03	0.10	0.53	19.04	13

to 3), whilst Fig. 8d, e show two final views of the uprooted tree.

The resulting $M - \varphi$ curve (Fig. 9) shows a complex nonlinear and irreversible behaviour, with progressive accumulation of permanent rotation at end of each unloading phase. The maximum values of the toppling resistance (point P in Fig. 9, with M_P = 9.15 kNm) was reached in cycle (3) for a rotation of 1.78°, relatively close to the limit condition of Wessolly and Erb equation (φ_L=1.914°). By considering the different loading–unloading cycles, it is also evident that increasing damage is induced into the system, since the average stiffness of the cycles is progressively reduced. Moreover, negligible rotation increment is observed between the first two cycles ($\Delta\varphi_{12} \approx 0$, as defined in Fig. 9), whilst an evident accumulation of permanent rotation $\Delta\varphi_{23}$ is present between the second and third cycle, probably owing to the activation of large displacement resisting mechanisms, mobilizing the pull-out resistance of the roots.

A deep and quantitative investigation of the progressive activation of such multiple failure mechanisms is beyond the purposes of the present work, since it would require detailed descriptions of the root geometry and of its local interaction with the soil (in general not available for practitioners during standard on-site pulling tests). The authors think, however, that investigating such loading–unloading response could be largely useful for the estimation of the toppling resistance of trees and for the definition of meaningful quantitative precursors of the inception of the global uprooting. In the following, consistently with the usual procedure consisting in a single monotonic loading path, only the envelope of the overall virgin loading curve will be considered, and the fitting procedure of Eqs. (1) and (3) will be applied by disregarding the unloading–reloading cycles. The collected experimental data have, however, been made here available even with the aim of promoting further investigations in future papers by other researchers.

4.5 Test F

The second pulling test was conducted on a tall tree (diameter of 30 cm), with an estimated height of 14 m. The pulling rope was fixed and a height of H=4.6 m from the ground and anchored at a distance of L=39.50 m (angle α=6.64°; Fig. 10). The same instrumental equipment described in Fig. 6 was employed, and the inclinometer was installed consistently with the reference system also shown in Fig. 10. The loading programme consisted again in several loading–unloading cycles at increasing amplitude, and the global $M - \varphi$ curve is shown in Fig. 11a. A complex nonlinear and irreversible behaviour is again evident, with important damaging effects (significant values of $\Delta\varphi_{12}$ and $\Delta\varphi_{23}$ are evident in Fig. 11a), and with the mobilization of a large toppling zone in the ground (Fig. 11c–d). During the loading phase of cycle (3), a long vertical crack opened on the compressed side of the trunk (Fig. 11b), which significantly modified the overall mechanical response of the system. The following part of the test (until the failure of the tree, consisted in a sudden trunk breakage, as shown in Fig. 11e) was then considered not representative of the toppling mechanism involving the root plate. Only the initial part of the test will then be considered for the fitting procedures, up to a rotation φ of about 1° (point P of Fig. 11a, with M_P = 21.48 kNm). The ultimate resistance is approximately 45 kNm (point U of Fig. 11a), which is, however, determined by trunk cracking and it cannot be considered representative of the toppling mechanism. As previously discussed for test E, only the envelope of the virgin loading curve up to point P will be considered in the following, and unloading–reloading cycles will be disregarded.

5 Interpretation of the experimental tests

5.1 Standard analysis

The results of the six tests were firstly analysed from the point of view of a professional user (i.e. with the aim of getting predictions of M_L values), by considering only "standard" non-destructive pulling tests. To this goal, tests A, B, C and D, together with the very initial part of the experimental curve of tests E and F (up to a rotation of 0.2°) were considered in the fitting procedures. The results are graphically summarized in Fig. 12a, b, and the list of all the fitting parameters is reported in Table 4 (the least squares method have been adopted for all the fitting procedures). The obtained best fitting values of the parameters allow an objective comparison between the two equations

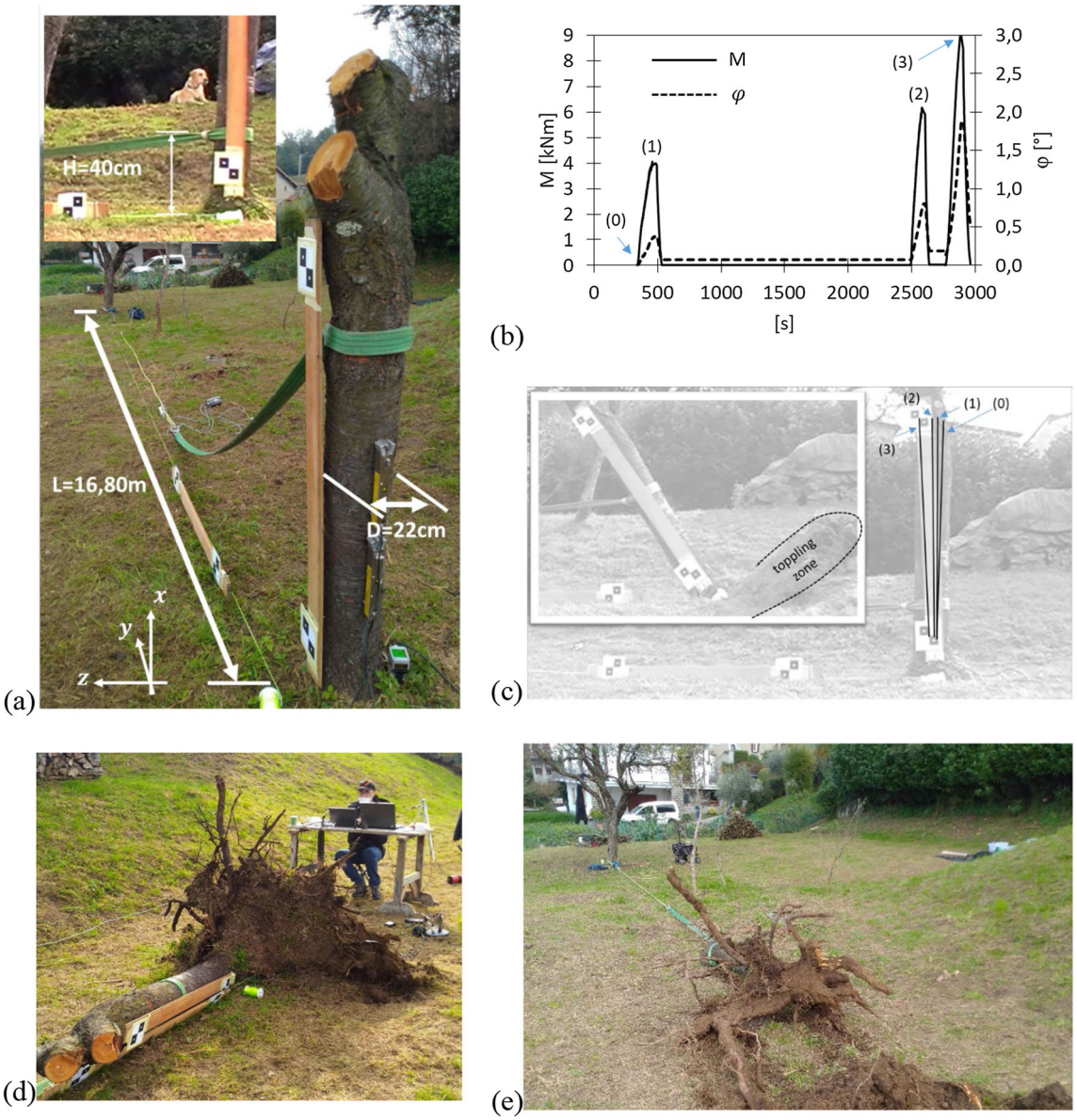

Fig. 8 **a** View of the experimental set up of test E; **b** load (solid line) and rotation (dashed line) records; **c** rotation of the tree and observed toppling mechanism; **d–e** views of the uprooted tree

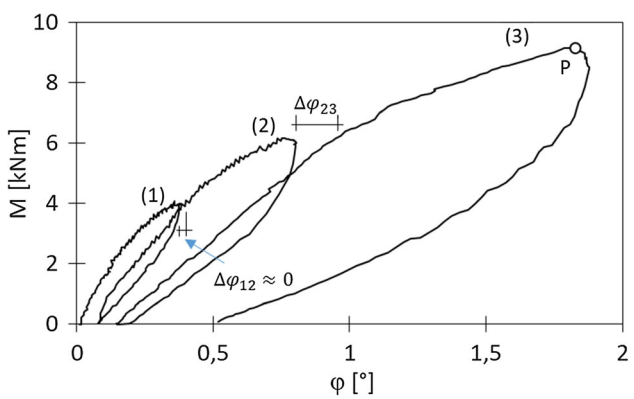

Fig. 9 $M - \varphi$ curve for test E

over the six tested experiments, and in particular, for the two newly proposed parameters φ_{70} and b, they give the reader an idea of the order of magnitude of the expected values for real-scale applications.

The experimental trend is qualitatively well reproduced in all the six cases by both equations, but it is evident how Wessolly and Erb model shows a less accurate quantitative agreement with the experimental data, in particular for tests A, B and D (characterized by larger-diameter values). For tests C, F and (although less evident) E some inaccuracies also appear. On the contrary, Eq. (3) accurately fits the experimental curves in all the six cases. These consideration are confirmed by the values of the root mean square

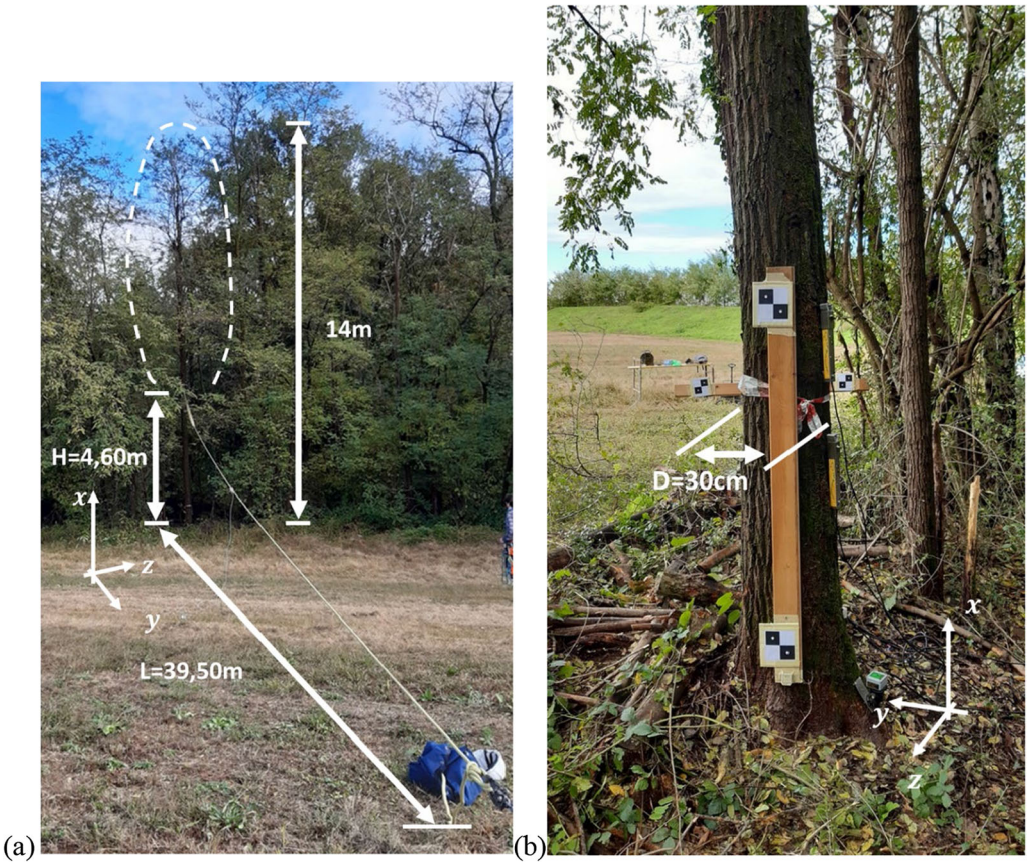

(a) (b)

Fig. 10 Test F: **a** view of the experimental set up and **b** detail of reference system

error (*RMSE*, also reported in Table 4) and computed for each test with respect to the measured rotation values φ. From these values, it can be observed how for tests E and F Eq. (3) significantly reduces the average errors of about 20 to 60% with respect to Eq. (1), whilst for large-diameter trees (tests, A, B, C and D) Eq. (3) increases the accuracy of about one order of magnitude with respect to Eq. (1). From a mechanical point of view, the accuracy in reproducing the experimental curve (even at low rotation values) is fundamental in view of a reliable estimation of the global rotational stiffness of the system. This quantity, in principle, is responsible for the correct modelling of advanced mechanical features (like second-order effects in large displacement computational schemes) or for optimizing the design of mechanical stabilizing interventions (like the design of ground anchors or rigid crutches).

With respect to toppling resistance, Eq. (1) leads in general to larger estimations of M_L with respect to Eq. (3), ranging between + 10% and + 76% (as shown in Fig. 12c, where the ratio of the two estimations is also plotted). With regard to parameter φ_{70}, relatively large values are obtained in particular for tests B and D (0.94° and 1.18°, respectively; see Table 4). For such trees, a hypothetic working condition characterized by $F_S = M_L/M_{70} = \sqrt{2}$ (≈ 1.4) is then associated with relevant rotation values (about 1°), potentially inducing irreversible damages to the roots. As a consequence, $F_S = 1.4$ cannot be considered in these cases as a "fully" safe condition, and larger values of the F_S should then be required. This proves how the choice of an operational values of the factor of safety should also depend on maximum tolerable rotation values. As far as parameter b is concerned, finally, values between 0.46 and 0.77 are obtained, with a slight decreasing trend for increasing diameter values.

5.2 Extended interpretation of tests E and F

The results of tests E and F can be further exploited by repeatedly running the fitting procedure over larger and larger portions of the experimental curve (always by considering the envelope of the monotonic part only). The idea is to test not only the "rapidity" and "stability" of the fitting values of M_L towards a safe operational value (which is a fundamental aspect for standard stability assessment procedures, given the limited portion of the curve which is usually investigated; see Fig. 1b), but also to derive some critical considerations about the mobilization of the resisting mechanisms over larger and larger parts of the toppling curve.

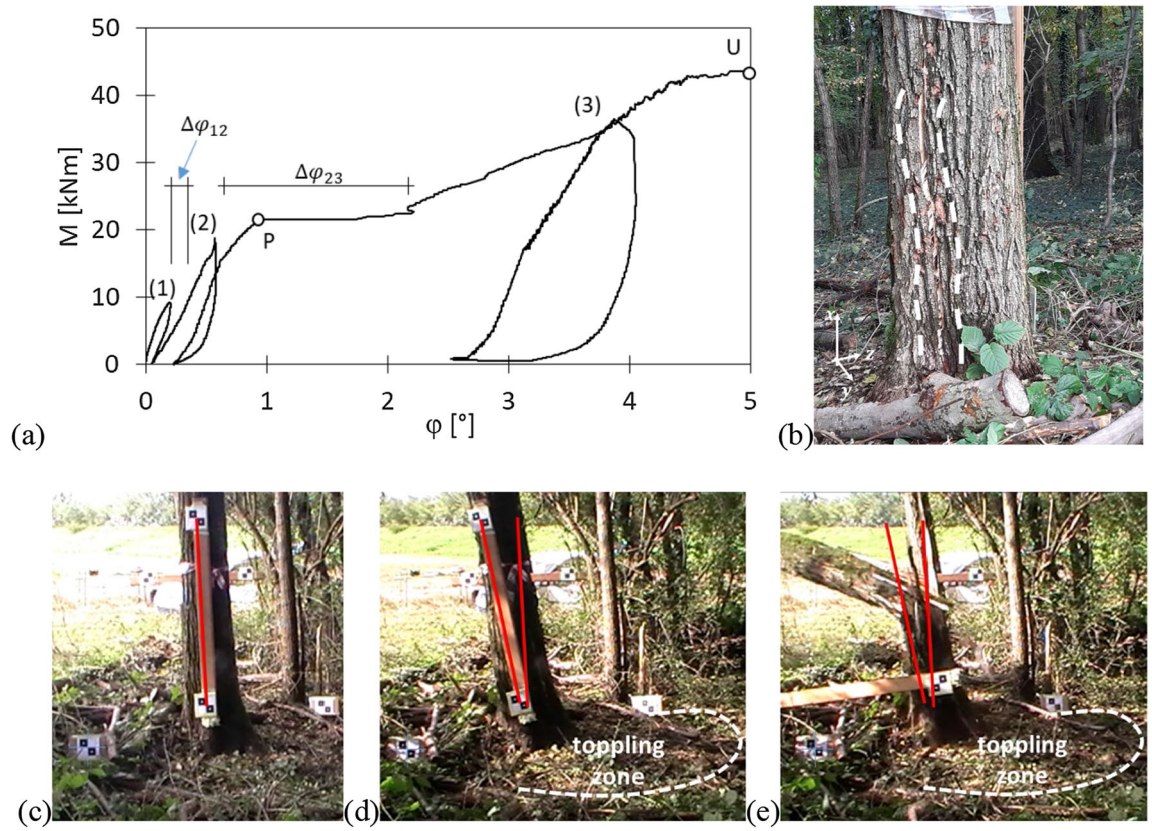

Fig. 11 **a** $M - \varphi$ curve for test F; **b** crack formation during the test; **c** view of the tree at the beginning of the test; **d–e** views of the tree just before and after the trunk breakage

Starting from this idea, the experimental data of tests E and F have been fitted both by Eqs. (1) and (3) by considering progressively increasing ranges of the mobilized resisting moment (expressed hereafter as a fraction of the quantity M_P and representing a sort of mobilization ratio).

Figure 13a shows the fitting values of parameter M_L for test E, both from Eqs. (1) and (3), when considering mobilization ratios between 20% (corresponding here to the standard interpretation of the pulling test) and 100% of M_P (i.e. by fitting the equations over toppling moments values between 0 and M_P). It proves a relatively stable estimation of M_L even for low mobilization ratios (with an average value of about 6.6 kNm between 20 and 50%), followed by an evident progressive increase in M_L for higher mobilization ratios (> 50% of M_P). This behaviour suggests that other failure mechanisms, different from the one initially captured by the fitting equation, are progressively activated at the level of the root plate. When considering 100% of mobilization ratio, the estimated value of M_L (about 11.62 kNm) significantly exceeds the observed M_P value. This can be explained by considering that M_L analytically represents the ultimate, asymptotic condition of an indefinitely stable and ductile mechanical response, who cannot account for large displacement and second-order effects, which are in general responsible of a progressive reduction of the toppling resistance. In this perspective, M_P must not be considered as an experimental validation for M_L values. As far as Eq. (1) is instead concerned, M_L values only show a slight continuously increasing trend, without any stable zone and without any evident distinction between the initial failure mechanism and higher-order ones.

From this comparison, it can be pointed out that (i) Eq. (3) gets in general more stable and safe estimations of M_L already for relatively low values of the applied toppling load, and (ii) it captures the progressive activation of higher-order failure mechanisms for increasing toppling loads. It must be observed in fact that one set of parameters (i.e. a set of values for M_L, φ_{70} and b) ideally allows to reproduce only one failure mechanism. A sharp change in the best fitting values for these three parameters for larger and larger mobilization ratios is then in principle associated with the activation of more complex mechanical phenomena.

Figure 13b plots the trends of parameters φ_{70} and b of Eq. (3), showing again relatively stable estimations up to a mobilization ratio of about 50% (average values of 0.54° and 1 are estimated for φ_{70} and b, respectively), followed

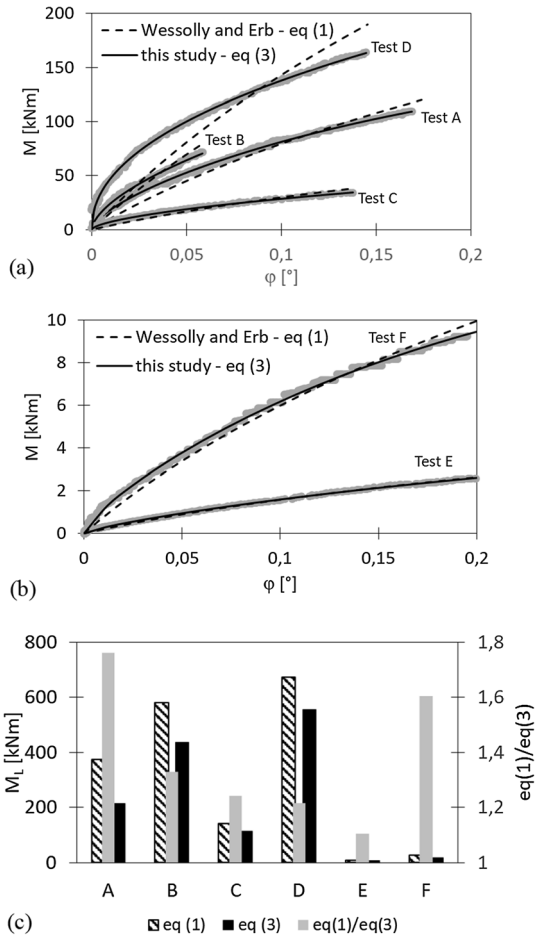

Fig. 12 Standard fitting procedure (grey dots represent the experimental data): **a** tests A, B, C and D; **b** tests E and F. **c** Comparison between the M_L values fitted from Eqs. (1) and (3)

by an increase in φ_{70} and a decrease in b. This is consistent with the fact that higher-order failure mechanisms are also associated with lower global stiffness (possibly due to irreversible damage processes taking place into the root system). Figure 13c, d shows instead the fitting curves for 50% and 100% of mobilization ratios, respectively. It is evident that for 50% mobilization ratio, both the curves accurately reproduce only the initial part of the experimental curve, with Wessolly and Erb equation giving a slight overestimation with respect to Eq. (3). For 100% mobilization ratio, Eq. (1) shows an initial stiffer response, followed by a less accurate flatter trend in the proximity of point P.

If test E represents an "ideal" pulling test on a healthy and completely pruned tree, perfectly fitting within the Wessolly and Erb calibration database, test F can be on the contrary considered as representative of a "real" case study regarding a complete tree with larger diameter, and characterized by weaker mechanical properties (collapse was in fact reached because of trunk failure, rather than because of uprooting). Nevertheless, similar considerations as those derived from Fig. 13 can be also derived for test F. Figure 14a, in fact, shows the estimated values of M_L with increasing mobilization ratios (the range 40–100% has been here explored), highlighting again rather stable estimations from Eq. (3) up to a mobilization ratio of about 60–70% (average M_L value of 17.76 kNm), followed by a pronounced increasing trend. Equation (1) gives instead a decreasing trend, which could be particularly unsafe for the pulling test interpretation, since it implies that higher ultimate toppling resistance values are estimated at low applied toppling loads. Figure 14b shows the evolution of parameters φ_{70} and b, respectively, again with rather constant values until mobilization ratios of about 60–70% (average values 0.38° and 0.8). The following marked increasing trend of φ_{70} accounts for a progressive reduction of the overall rotational stiffness, probably due to increasing damaging levels in the root plate. Parameter b, instead, shows only a slow decreasing trend, meaning that the experimental curve is always characterized by a major curvature with respect to Wessolly and Erb equation. Finally, for the sake of completeness, in Fig. 14c, d the two fitting curves for 50% and 100% mobilization ratio, respectively, are plotted.

Although applied here to only two experimental tests, this method (consisting in running the fitting procedure

Table 4 List of fitting parameter of experimental tests and of the M_P values of tests *E* and *F*

		Wessolly and Erb — Eq. (1)		This study — Eq. (3)			
Test	M_P[kNm]	M_L[kNm]	*RMSE*[°]	M_L[kNm]	φ_{70}[°]	b[−]	*RMSE*[°]
A	–	374.46	8.03E-03	212.83	0.35	0.65	1.41E-03
B	–	580.89	4.01E-03	436.94	0.94	0.60	4.88E-04
C	–	140.81	8.47E-03	113.46	0.76	0.60	8.48E-04
D	–	673.80	1.41E-02	554.77	1.18	0.46	8.64E-04
E	9.15	7.44	6.23E-03	6.73	0.64	0.77	5.25E-03
F	21.48	28.13	5.31E-03	17.53	0.37	0.75	2.02E-03

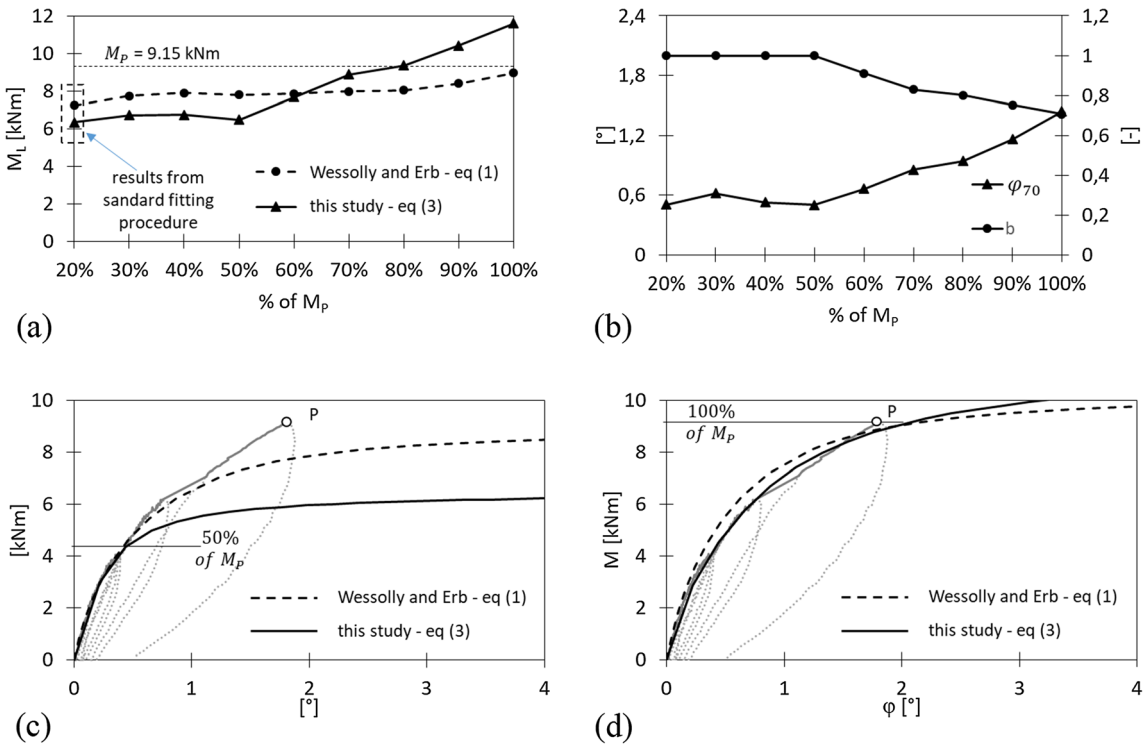

Fig. 13 Fitting of Eqs. (1) and (3) over the experimental data from test E for different mobilization ratios. **a** values of M_L; **b** values of φ_{70} and b; **c–d** predicted curves fitted over 50% and 100% of M_P, respectively

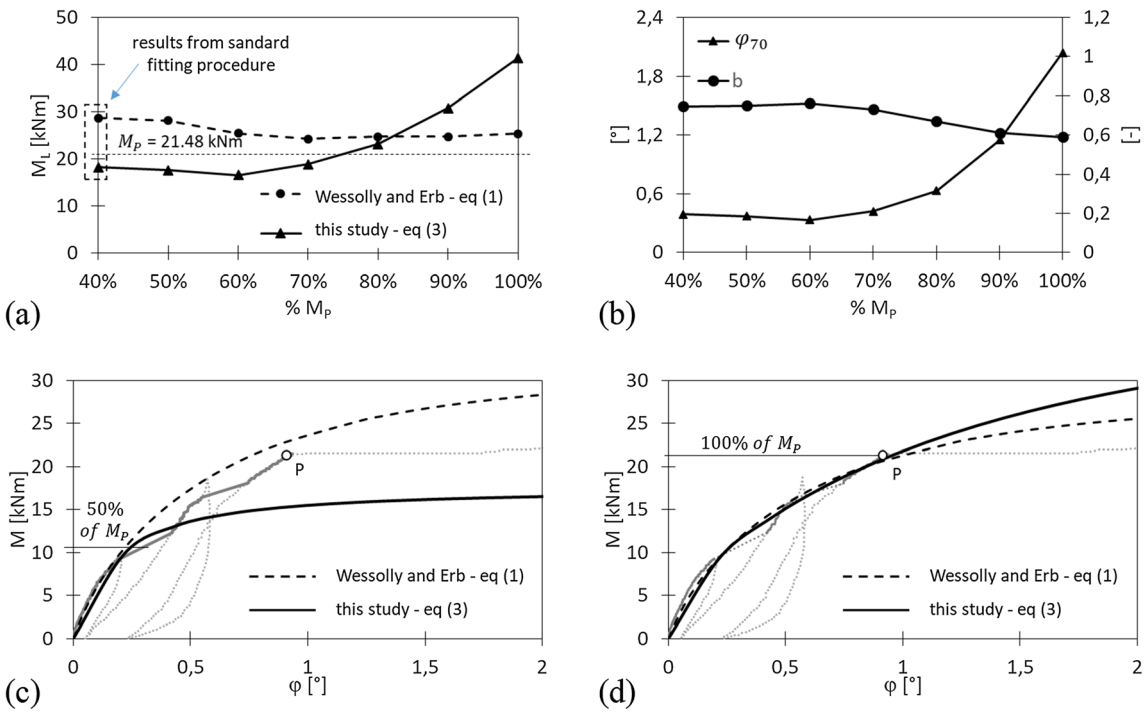

Fig. 14 Fitting of Eqs. (1) and (3) over the experimental data from test F for different mobilization ratios. **a** values of M_L; **b** values of φ_{70} and b; **c–d** predicted curves fitted over 50% and 100% of M_P, respectively

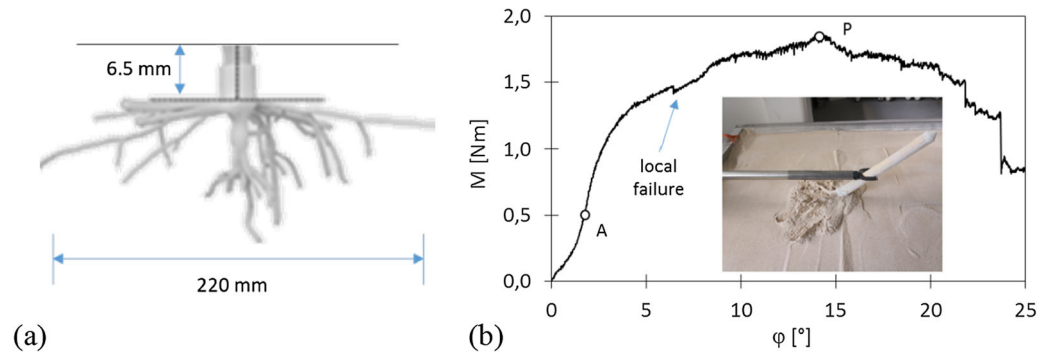

Fig. 15 **a** View of the 3D printed root model and **b** test results. Modified from [8]

over a progressively increasing set of experimental data for larger and larger mobilization ratios) has a general validity and it could possibly inspire new real-time interpretative codes to be run directly during the execution of standard pulling tests.

5.3 Small-scale pulling tests

The capability of the two equations to capture significantly different size effects (even beyond the proper range of applicability of Wessolly and Erb equation), was also tested by considering a seventh experimental pulling test on a small-scale tree prototype. The aim is not to provide practical scaling laws for the values of the governing parameters, but to show how the proposed Eq. (3) can accurately be employed both to large- and small-diameter trees. A 1:20 small-scale 1-g displacement-controlled laboratory test taken from the literature [8] was considered, run on a 3D printed root model, with a global diameter of 220 mm and embedded 6.5 mm below the ground level (Fig. 15a). The soil was a mixture of 70% dry sand and 30% silt, with a relative density of about 48%. The dry unit weight of the soil was γ_{dry}=16.5 kN/m^3 and a critical state friction angle, derived from direct shear tests, is $\phi' = 38°$ (further details can be found in the cited paper). The test showed a marked nonlinear behaviour, with a peak toppling moment M_P = 1.86 Nm at a rotation of 13° (point P of Fig. 15b) and followed by a strength reduction, witnessing a global fragile behaviour of the system at large rotation values. A minor local failure phenomenon is

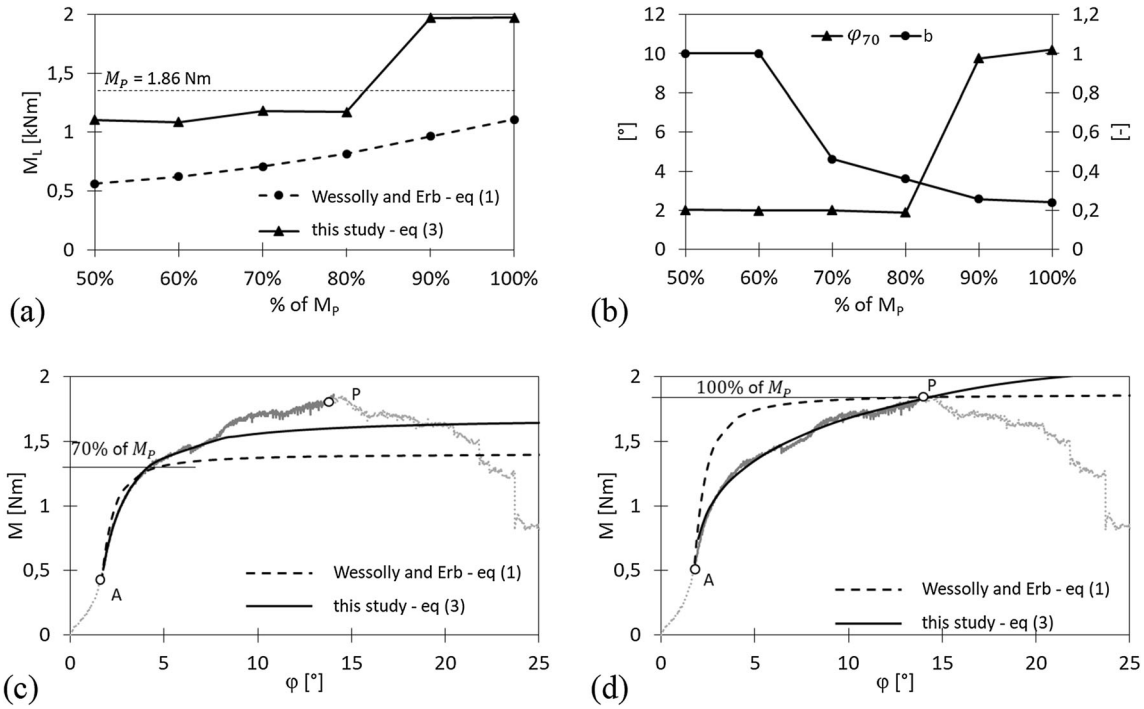

Fig. 16 Fitting of Eqs. (1) and (3) over the experimental data from [8] for different mobilization ratios. **a** Values of M_L; **b** values of φ_{70} and b; **c**–**d** predicted curves fitted over 70% and 100% of M_P, respectively

observed for a rotation of about 6.46°, beyond which a secondary failure mechanism is apparently activated. It is worth noting that the initial part of the curve (from the origin up to point A, corresponding to a toppling moment of 0.51 Nm) is characterized by a significant stiffening effect, probably due to soil disturbance in model preparation, and it will not be considered in the following fitting procedures.

The results of the interpolation by means of Eqs. (1) and (3) are summarized in Fig. 16, following the same approach already discussed for tests E and F (in this case, for the sake of significance with respect to the lower limit represented by point A, only mobilization ratios larger than 50% of M_P have been considered). Equation (3), again, shows stable predictions both in terms of M_L and φ_{70} for a relatively wide range of mobilization ratios (with average values of about 1.1 Nm and 2°; see Fig. 16a, b, respectively), followed by a marked increase for higher mobilization ratios (> 80%), consisting with the activation of a possible secondary failure mechanism. Parameter b shows instead a marked decrease (from 1 to about 0.2). On the contrary, M_L values from Eq. (1) show only a minor increasing trend for increasing mobilization ratios, with severe underestimations (about 30–50%) with respect to the values obtained by means of Eq. (3). Finally, the two fitting curves are also reported in Fig. 16c, d for 70% and 100% of mobilization ratios, respectively. It can be noted that Wessolly and Erb equation generally shows initially a stiffer mechanical response, very evident even when the complete loading curve (i.e. mobilization ratio of 100%) is considered. This is due to the fact that, as initially pointed out in Sect. 2, a fixed value φ_{70}=0.653° is implicitly assumed in Eq. (1), preventing the possibility to capture significant size effects.

6 Conclusions

In the paper, several pulling tests on trees are discussed (both considering real-scale and small-scale experimental results, and by adopting monotonic and cyclic loading schemes), and it has been observed how the general mechanical response is characterized by a complex, nonlinear and irreversible moment–rotation curve. The experimental data revealed that the toppling mechanism is a complex process, consisting in the progressive activation of several and subsequent resisting mechanisms (characterized by increasing strength and decreasing stiffness), possibly corresponding with the mobilization of second-order and large displacement effects. The prediction of the ultimate toppling resistance (especially when, as in real cases, the tests are limited to very low rotation values) is then a complex problem, that can hardly be described by a unique global fitting equation and requires in principle a multi-mechanism approach.

Despite this limitation, in the paper a new interpretative equation is proposed, extending and enriching the usual Wessolly and Erb equation. In particular, a meaningful mechanical relationship is here introduced for the moment–rotation curve, thought as a single-d.o.f. rotational system. With respect to the traditional "capacity-based" approach, the presented framework allows to move towards innovative "performance-based" approaches, characterizing the system not only in terms of its toppling resistance, but also in terms of a reference rotation value under a prescribed working condition (represented here by parameter φ_{70}). As a result, standard stability assessment procedures (usually based only on the definition of a global factor of safety against toppling) can be enriched by the evaluation of the corresponding rotation, to be compared with a maximum tolerable value for the tree.

In the considered cases, the new equation accurately fit the experimental data and it also correctly captured important size effects. For standard predictions, Wessolly and Erb equation showed a general tendency at overestimating the values of the toppling resistance with respect to the new proposed equation, which can then be considered more conservative. When considering "extended" predictions on progressively increasing values of the mobilization ratios, the new equation proved to rapidly and stably provide safe estimations of the ultimate toppling resistance (at least of the first failure mechanism) and to adaptively capture the progressive activation of higher-order failure mechanisms during the execution of the tests. This property is of particular practical interest, since it can significantly help practitioners in the interpretation of the pulling tests, for example, by adopting innovative real time fitting procedures to be run during the execution of the test. It is worth noting, finally, that the new equation does not require any significant additional computational cost to the user (standard least square fitting procedures were in all cases adopted throughout the paper).

At authors' judgement, however, the development of a new, mechanically meaningful interpretative framework for the moment–rotation curve of a tree has also the important outcomes of (i) pushing the scientific research towards the definition of more reliable relationships with soil mechanical properties and root typologies, and (ii) improving the design procedures of sustainable structural stabilizing interventions on trees. It is authors' hope that the present paper can give a contribution in these directions, and promote the scientific and professional debate on these topics.

Acknowledgements The authors want to warmly acknowledge Mr. Luigi Panzeri and Mrs. Carla Castiglioni for having kindly agreed to

the execution of the pulling tests E and F, and Dr. Nicoletta Fusi for the grain size distributions of the two samples. The support provided by Agro Services s.r.l. and the Scottish Research Partnership in Engineering (SRPe), through the Industry Doctorate Programme research grant SRPe-IDP/011, is also acknowledged.

Funding Open access funding provided by Politecnico di Milano within the CRUI-CARE Agreement.

Data availability The datasets generated during and/or analysed during the current study are available from the corresponding author on reasonable request.

References

1. AIDTPG (2015) Linee guida per la gestione dei patrimoni arborei pubblici (nell'ottica del Risk Management). Associazione Italiana Direttori e Tecnici Pubblici Giardini, Editoriale Sometti (Mantova), p 66
2. BBC (2022) Storm Arwen damaged 16 million trees. https://www.bbc.co.uk/news/uk-scotland-south-scotland-60926691
3. Blackwell PG, Rennolls K, Coutts MP (1990) A root anchorage model for shallowly rooted Sitka spruce. Forestry 63:73–91. https://doi.org/10.1093/forestry/63.1.73
4. British Standards 3998 (2010) "Recommendations for tree work"
5. Cao J, Tamura Y, Yoshida A (2012) Wind tunnel study on aerodynamic characteristics of shrubby specimens of three tree species. Urban For Urban Green 11:465–476. https://doi.org/10.1016/j.ufug.2012.05.003
6. Crook MJ, Ennos AR (1996) The anchorage mechanics of deep rooted larch, Larix europea × L. japonica. J. Exp. Botany 47(10):1509–1517
7. Cucchi V, Meredieu C, Stokes A et al (2004) Root anchorage of inner and edge trees in stands of maritime pine (Pinus pinaster Ait.) growing in different podzolic soil conditions. Trees 18:460–466. https://doi.org/10.1007/s00468-004-0330-2
8. Dattola G, Ciantia MO, Galli A, Blyth L, Zhang X, Knappet JA, Castellanza R, Sala C, Leung AK (2020) A macroelement approach for the stability assessment of trees. Lecture Notes Civil Eng 40:417–426
9. Dupuy L, Fourcaud T, Stokes A (2005) A numerical investigation into the influence of soil type and root architecture on tree anchorage. Plant Soil 278:119–134. https://doi.org/10.1007/s11104-005-7577-2
10. Défossez P, Veylon G, Yang M, Bonnefond JM, Garrigou D, Trichet P, Danjon F (2021) Impact of soil water content on the overturning resistance of young Pinus Pinasterin sandy soil. For Ecol Manage 480:118614
11. Fakopp (2020) Manual for the pulling test. Fakopp Enterprise (Hungary), http://www.fakopp.com
12. Galli A (2020) Macroelement approaches for geotechnical problems: a promising design frame- work? Rivista Italiana di Geotecnica 54(2):27–49
13. Galli A, Maiorano RMS, di Prisco C, Aversa S (2017) Design of slope-stabilizing piles: from ultimate limit state approaches to displacement based methods. Rivista Italiana di Geotecnica 51(3):77–93
14. Gromke C, Ruck B (2008) Aerodynamic modelling of trees for small-scale wind tunnel studies. Forestry 81:243–258. https://doi.org/10.1093/forestry/cpn027
15. Guitard DGE, Castera P (1995) Experimental analysis and mechanical modelling of windinduced tree sways. In: Coutts MP, Grace J (eds) Wind and trees: 182–194. https://doi.org/10.1017/cbo9780511600425.010
16. Martinez A, DeJong J, Akin I, Aleali A, Arson C, Atkinson J, Bandini P, Baser T, Borela R, Boulanger R, Burrall M et al (2021) Bio-inspired geotechnical engineering: Principles, current work, opportunities and challenges. Géotechnique 72(8):687–705
17. Mattheck C, Breloer H (1998) La stabilità degli alberi. Fenomeni meccanici e implicazioni legali dei cedimenti degli alberi. Il Verde Editoriale, p 281
18. Morgan RP, Rickson RJ (2003) Slope Stabilization and Erosion Control: A Bioengineering Approach. Taylor & Francis
19. Motta R, Ascoli D, Corona P, Marchetti M, Vacchiano G (2018) Selvicoltura e schianti da vento Il caso della "tempesta Vaia." Forest@ Rivista di Selvicoltura ed Ecologia Forestale 15:94–98
20. Nicoll BC, Gardiner BA, Rayner B, Peace AJ (2006) Anchorage of coniferous trees in relation to species, soil type, and rooting depth. Can J For Res 36(7):1871–1883. https://doi.org/10.1139/X06-072
21. Nova R, Montrasio L (1991) Settlements of shallow foundations on sand. Géotechnique 41:243–256
22. Priestley MJN, Calvi GM, Kowalsky MJ (2007) Direct Displacement-Based Seismic Design. IUSS Press, Pavia
23. di Prisco C, Flessati L, Frigerio G, Galli A (2020) Mathematical modelling of the mechanical response of earth embankments on piled foundations. Geotechnique 70(9):755–773
24. Raimondi A, Becciu G (2021) Performance of green roofs for rainwater control. Water Resour Manage 35(1):99–111
25. Raimondi A, Marchioni M, Sanfilippo U, Becciu G (2020) Infiltration-exfiltration systems design under hydrological uncertainty. WIT Transact Built Environ 194:143–154
26. Sani L (2017) Statica delle strutture arboree. Gifor, ISBN-13: 979-–1220016698, p 945
27. Satterthwaite D (2007) Adapting to climate change in urban areas: the possibilities and constraints in low-and middle-income nations (1). Iied
28. Schiechtl HM (1985) FAO watershed management field manual: vegetative and soil treatment measures (No. 1–5). Food and Agriculture Org
29. Schwarz M, Cohen D, Or D (2010) Root-soil mechanical interactions during pullout and failure of root bundles. J Geophys Res Earth Surf 115:1–19. https://doi.org/10.1029/2009JF001603
30. Sellier D, Fourcaud T (2009) Crown structure and wood properties: influence on tree sway and response to high winds. Am J Bot 96:885–896. https://doi.org/10.3732/ajb.0800226
31. Siegert B (2013) Comparative analysis of tools and methods for the evaluation of tree stability: results of a field test in Germany. Arborist News 22(2):26–31
32. Stokes A, Douglas GB, Fourcaud T, Giadrossich F, Gillies C, Hubble T et al (2014) Ecological mitigation of hillslope instability: ten key issues facing researchers and practitioners. Plant Soil 377(1):1–23
33. Switala BM, Wu W, Wang S (2019) Implementation of a coupled hydro-mechanical model for root-reinforced soils in finite element code. Comput Geotech 112:197–203

34. Wessolly L, Erb M (1998) Handbuch der Baumstatik und Baumkontrolle. Patzer, Berlin
35. Wit Motion (2019) WT901C digital attitude sensor SPECIFICATION, htttp://www.wit-motion.com
36. Yang M, Défossez P, Danjon F, Fourcaud T (2014) Tree stability under wind: simulating uprooting with root breakage using a finite element method. Ann Bot 114:695–709. https://doi.org/10.1093/aob/mcu122
37. Yang M, Défossez P, Danjon F, Fourcaud T (2018) Analyzing key factors of roots and soil contributing to tree anchorage of Pinus species. Trees Struct Funct 32:703–712. https://doi.org/10.1007/s00468-018-1665-4
38. Zhang X, Knappett JA, Leung AK et al (2020) Small-scale modelling of root-soil interaction of trees under lateral loads. Plant Soil. https://doi.org/10.1007/s11104-020-04636-8
39. Zhang X, Knappett JA, Leung AK, Ciantia MO, Liang T, Nicol BC (2022) Centrifuge modelling of root-soil interaction of laterally loaded trees under different loading conditions. Article in press, Géotechnique